0.12); (+)-**3b** gave rise to (+)-(3*R*)-**1b** (27% yield) $[\alpha]^{20}_D$ +23.8° (*c* 0.13).

The C-3 and C-4 chiralities of (−)-**3a,b** followed from their enantiomeric relationships to those of the corresponding (+) stereoisomers. The overall absolute configuration assignments are summarized in Schemes II and III.

Acknowledgment. Support by the Natural Science and Engineering Council of Canada is gratefully acknowledged. We are also indebted to Hoffmann-La Roche for financial aid and a generous gift of the enzyme and to Professor Keith Dorrington for providing such ready access to his Cd instrument.

Registry No. (±)-**1a**, 84583-08-4; (−)-(3*S*)-**1a**, 84622-33-3; (+)-(3*R*)-**1a**, 84622-39-9; (±)-**1b**, 84583-10-8; (−)-(3*S*)-**1b**, 84622-36-6; (+)-(3*R*)-**1b**, 84622-41-3; (±)-**2a**, 84583-11-9; (+)-(3*S*,4*S*)-**2a**, 84622-34-4; (±)-**2b**, 84583-13-1; (+)-(3*S*,4*S*)-**2b**, 84622-37-7; (±)-**3a**, 84583-12-0; (+)-(3*R*,4*S*)-**3a**, 84622-35-5; (−)-(3*S*,4*R*)-**3a**, 84622-40-2; (±)-**3b**, 84583-14-2; (+)-(3*R*,4*S*)-**3b**, 84622-38-8; (−)-(3*S*,4*R*)-**3b**, 84622-42-4; **5**, 84583-06-2; 3-carbomethoxy-3-methyltetrahydrothiopyran-4-one, 84583-07-3; 3-carbomethoxy-3-ethyltetrahydrothiopyran-4-one, 84583-09-5; alcohol dehydrogenase, 9031-72-5.

Electronic Structure and Reactivity of Homobarrelene Derivatives

Rolf Gleiter,*† Michael C. Böhm,† Armin de Meijere,‡ and Thomas Preuss‡

Institut für Organische Chemie der Universität Heidelberg, D-6900 Heidelberg, and Institut für Organische Chemie und Biochemie der Universität Hamburg, D-2000 Hamburg, West Germany

Received August 10, 1982

The He(I) photoelectron (PE) spectra of homobarrelene (**1**), *endo,exo*- and *exo,exo*-dihomobarrelene (**2** and **3**) and trihomobarrelene (**4**) have been investigated. The first bands in the PE spectra of **1**–**4** are assigned on the basis of MINDO/3 and INDO calculations. The localized orbitals derived from INDO calculations are used to discuss the through-bond and through-space interaction present in **1**–**4**. The results of this analysis are used to rationalize the stereochemistry observed for the reaction of **1** and the hetero derivatives **6** and **7** with carbene, nitrene, and peracids.

In recent years the interaction between the valence orbitals of a cyclopropane moiety and π bonds has been studied extensively by means of low-energy photoelectron (PE) spectroscopy.[1-8] It has been demonstrated that the interaction between the π system and the three-membered-ring fragment critically depends on the orientation between both units and that a through-space and a through-bond[9] coupling mechanism can be used to describe the interactions.

In this paper we analyze the He(I) photoelectron (PE) spectra of various barrelene derivatives containing a three-membered ring instead of a double bond. The hydrocarbons are homobarrelene (**1**), *endo,exo*- and *exo,exo*-dihomobarrelene (**2** and **3**), and trihomobarrelene (**4**). The PE spectra of **1**–**4** are compared with the spectrum of barrelene (**5**).[10]

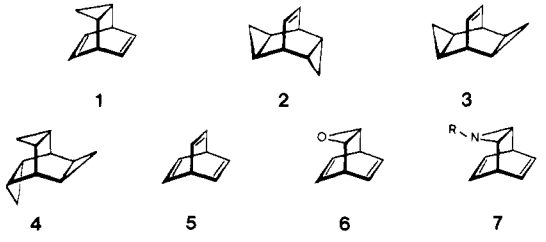

A second aim of this paper is to evaluate the magnitude of through-space and through-bond interactions in these species and to rationalize the strikingly different regiochemistry of the cheletropic cycloadditions of methylene, nitrene, and "oxene" (from *m*-chloroperbenzoic acid) to **1**, **6**, and **7**.

Photoelectron Spectra

The PE spectra of **1**–**4** are shown in Figure 1, and the vertical ionization potentials are collected in Table I. To assign the first bands in the PE spectra of **1**–**4**, we assume the validity of Koopmans' theorem[11] shown in eq 1. This

$$I_{V,J}{}^{K} = -\epsilon_J \qquad (1)$$

assumption allows us to compare the measured vertical ionization potentials, $I_{V,J}$, with calculated orbital energies, ϵ_J, using molecular orbital (MO) models. To derive the orbital energies, we use a recently developed INDO approximation[12] and the MINDO/3[13] method. The geometries of **1**–**5** correspond to the energy minimum obtained by the MINDO/3 method by optimizing the total energy with respect to the geometrical variables.

The PE spectrum of **5**[10] shows two bands below 10 eV which have been assigned to ionization events from the π

† Heidelberg.
‡ Hamburg.

(1) Gleiter, R. *Top. Curr. Chem.* **1979**, *86*, 197.
(2) de Meijere, A. *Angew. Chem.* **1979**, *91*, 867; *Angew. Chem., Int. Ed. Engl.* **1979**, *18*, 809. Klessinger, M.; Rademacher, P. *Angew. Chem.* **1979**, *91*, 885; *Angew. Chem., Int. Ed. Engl.* **1979**, *18*, 826.
(3) Bischof, P.; Heilbronner, E.; Prinzbach, H.; Martin, H.-D. *Helv. Chim. Acta* **1971**, *54*, 1072.
(4) Gleiter, R.; Heilbronner, E.; de Meijere, A. *Helv. Chim. Acta* **1971**, *54*, 1029.
(5) (a) Bruckman, P.; Klessinger, M. *Chem. Ber.* **1974**, *107*, 1108. (b) Bruckman, P.; Klessinger, M. *Angew. Chem.* **1972**, *84*, 543; *Angew. Chem., Int. Ed. Engl.* **1972**, *11*, 524.
(6) Askani, R.; Gleiter, R.; Heilbronner, E.; Hornung, V.; Musso, H. *Tetrahedron Lett.* **1971**, 4461.
(7) Bischof, P.; Gleiter, R.; Heilbronner, E.; Hornung, V.; Schröder, G. *Helv. Chim. Acta* **1970**, *53*, 1645.
(8) Prins, I.; Verhoeven. J. W.; de Boer, T. J.; Worrell, C. *Tetrahedron* **1977**, *33*, 127.
(9) Hoffmann, R.; Imamura, A.; Hehre, W. J. *J. Am. Chem. Soc.* **1968**, *90*, 1499. Hoffmann, R. *Acc. Chem. Res.* **1971**, *4*, 1. Gleiter, R. *Angew. Chem.* **1974**, *86*, 770; *Angew. Chem., Int. Ed. Engl.* **1974**, *13*, 696.
(10) Haselbach, E.; Heilbronner, E.; Schröder, G. *Helv. Chim. Acta* **1971**, *54*, 153.
(11) Koopmans, T. *Physica (Utrecht)* **1934**, *1*, 104.
(12) Böhm, M. C.; Gleiter, R. *Theor. Chim. Acta* **1981**, *59*, 127.
(13) Bingham, R. C.; Dewar, M. J. S.; Lo, D. H. *J. Am. Chem. Soc.* **1975**, *97*, 1285. We used the MINDO/3 UHF version written by Bischof.[14]
(14) Bischof, P. *J. Am. Chem. Soc.* **1976**, *98*, 6844.

0022-3263/83/1948-0796$01.50/0

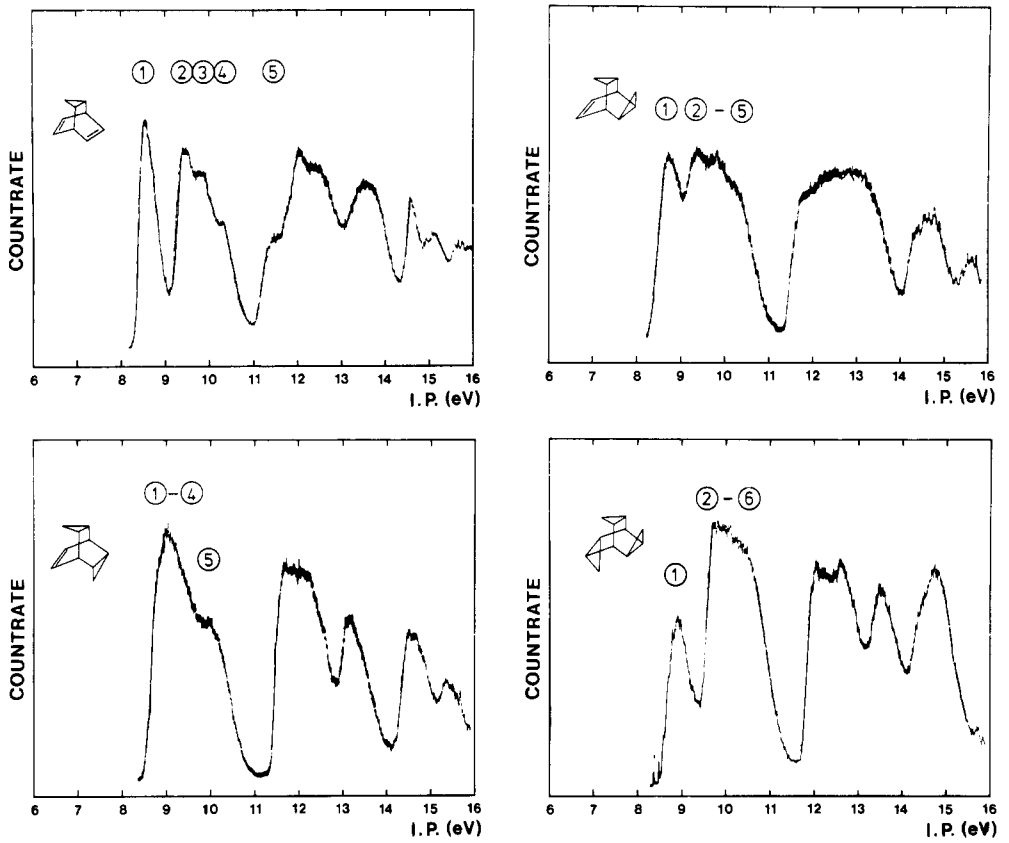

Figure 1. He(I) spectra of 1–4.

Table I. Comparison between the First Vertical Ionization Potentials, $I_{V,J}$, and Calculated Orbital Energies, ϵ_J, by Means of the MINDO/3 and INDO Method for 1–5

compd	band	$I_{V,J}$, eV	assignment[a]	$-\epsilon_J$, eV MINDO/3	$-\epsilon_J$, eV INDO
1 (C_s)	1	8.50	15a′	9.04	9.31
	2	9.28	14a′	9.26	10.10
	3	9.70	13a′	9.46	11.03
	4	10.17	8a″	9.57	11.05
2 (C_s)	1	8.64	17a′	9.29	9.53
	2	9.3	16a′	8.97	10.44
	3	9.7	9a″	9.51	11.08
	4	10.1	8a″	9.88	11.42
3 (C_{2v})	1		$7b_1$	9.32	9.77
	2	9.0	$6b_1$	9.39	10.37
	3		$10a_1$	9.19	10.83
	4	9.9	$6b_2$	9.73	10.98
			$3a_2$	9.61	11.64
4	1	8.8	7a′	8.85	10.08
	2	9.7	6e′	9.58	10.92
	3	10.1	3e″	9.64	11.36
5	1	8.23	$1a_2'$	8.94	9.00
	2	9.65	4e′	9.40	10.44

[a] The numbering refers to the valence orbitals only.

MO's $1a_2'$ and 4e′. For reasons of symmetry $1a_2'$ does not interact with the σ frame while 4e′ is considerably destabilized by σ/π interaction.[10] The computational results in Table I clearly indicate that the MINDO/3 procedure overestimates the σ/π interaction. The predicted energy gap $1a_2'$–4e′ of 0.46 eV has to be compared with the experimental value of 1.42 eV. This split is very well reproduced, however, by the INDO model (see Table I).

In case of 1 we expect four ionization events in the outer valence region, two of predominant π character and two of the Walsh[15] type, the symmetric and antisymmetric W_S and W_A linear combinations which are schematically shown below. For the ionization potential corresponding

$$W_S = \frac{1}{2^{1/2}}(\phi_1 + \phi_2) \qquad W_A = \frac{1}{6^{1/2}}(\phi_3 - \phi_1 + \phi_2)$$

to W_A we expect a value about 10 eV from the comparison with the PE spectra of 8–11.[1,3] A comparison of the PE spectra of 10 and 11 shows that only in the case of 11 is a significant interaction between π and W_S present. The resonance integral for this interaction nearly reaches the value of π/π coupling while the interaction between π and

(15) Walsh, A. D. *Nature (London)* **1947**, 150, 167, 712; *Trans. Faraday Soc.* **1949**, *45*, 179.

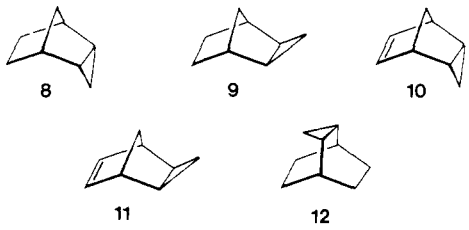

W_S is minute in **10**.[3] Thus the two double bonds in **1** should be differently influenced by the cyclopropane moiety.

As anticipated, the PE spectrum of **1** shows four maxima in the lower energy region (bands 1–4) which have been discussed previously.[5,6] The INDO results in Table I suggest assignment of the first two bands to ionization events from MO's with dominant π character (15a′ and 14a′). The next two bands are assigned to the Walsh-type orbitals 13a′ and 8a″. The values predicted by the INDO method are very close to the experimental ones; i.e., the magnitudes of through-bond and through-space interaction are treated properly. As was already encountered in the case of **5**, MINDO/3 overestimates through-bond interaction, and thus the energy differences between the bands are predicted to be too small.

In the PE spectrum of **2** the first band is separated from a series of strongly overlapping bands. A comparison between the ionization potential (8.64 eV) of the first band and that of bicyclo[2.2.2]octene (9.05 eV)[16] suggests that the first peak is due to the ionization from the π orbital 17a′. This assignment is in line with the INDO result given in Table I. The second peak (9.3 eV) corresponds to the symmetrical Walsh orbital of the *exo*-cyclopropyl group ($W_S(1)$) which shows negligible interaction with the π bond. This assignment is based on the comparison with the first band in the PE spectrum of **12** which is found at 9.3 eV.[3] Bands 3 and 4 of **2** can be assigned to ionization processes from linear combinations of symmetrical and antisymmetrical Walsh orbitals localized at both rings.

In **3** we encounter only two peaks below 10 eV with the approximate intensity ratio of 4:1. This is anticipated since we expect only a relatively small interaction between the two exo-oriented rings and the double bond. The first maximum at 9.0 eV must be assigned to four overlapping ionization events from the π-type MO 7b and from the three Walsh-type combinations ($6b_1(W_S^+)$, $10a_1(W_S^+)$, $6b_2(W_A^+)$) shown below. The second peak (9.9 eV) is

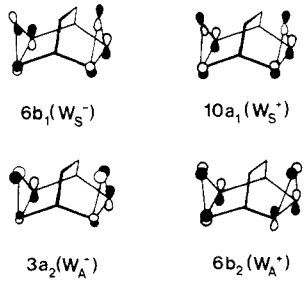

assigned to $3a_2$, the antibonding linear combination of the antisymmetric Walsh orbital, W_A^-. The energy difference between bands 1 and 4 is in line with the energy interval predicted for the highest occupied four MO's by INDO. Also the experimental separation between the two maxima of 0.9 eV is close to the calculated energy difference between the center of gravity of $7b_1$, $6b_1$, $10a_1$, $6b_2$, and $3a_2$

(16) Bischof, P.; Hashmall, J. A.; Heilbronner, E.; Hornung, V. *Helv. Chim. Acta* **1969**, *52*, 1745.

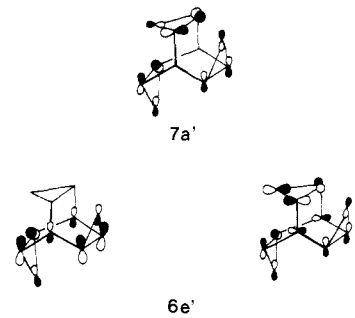

Figure 2. Schematic representation of the highest occupied molecular orbitals of **4**.

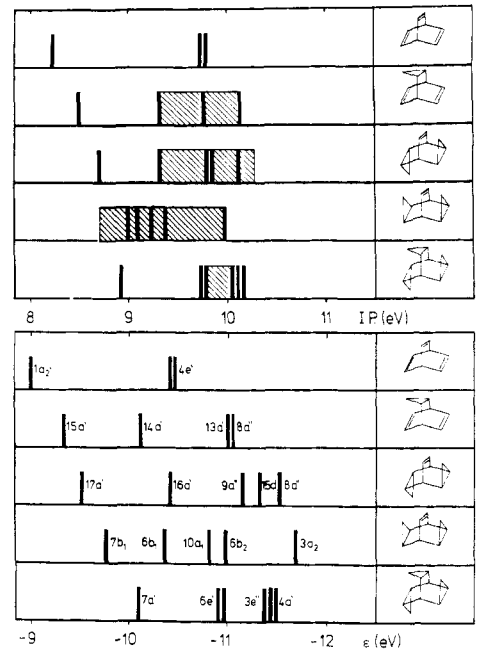

Figure 3. Comparison between the first bands of the PE spectra of **1**–**5** (top) with results of INDO calculations (bottom).

which is found to be 1.2 eV. The PE spectrum of **4** shows two maxima below 11 eV. The first band at 8.8 eV is clearly separated from strongly overlapping bands around 10 eV. The first band is assigned to MO 7a′, the antibonding linear combination of the symmetric Walsh orbitals (see Figure 2). The broad maximum around 10 eV most probably corresponds to ejections from the MO's 6e′ (shown in Figure 2) as well as 3e″ and 4a′. This assignment is based on the INDO and MINDO/3 results (see Table I).

A comparison was made of the bands (Figure 3) recorded in the low-energy region (below 11 eV) of the PE spectra with molecular orbital energies calculated by the INDO model.[12] It is seen that this semiempirical LCAO model gives an accurate description of the sequence and energy differences of the various ionization events in the whole series. Thus the INDO model is suitable to derive the through-bond and through-space interaction in **1**–**5**.

Magnitude of "Through-Space" and "Through-Bond" Interactions in Barrelene Homologues

To understand the stereoselectivity of **1**, **6**, and **7** toward electron-deficient species, we have to analyze the magnitude of the through-space and through-bond interaction in these examples. The method we use is close to the approach originally developed by Heilbronner and Schmelzer.[17] In the first step the occupied canonical

Hartree–Fock (HF) orbitals (CMO's) φ_j of the diagonal Fock matrix are transformed into a set of localized MO's (LMO's) λ_j by means of the Edmiston–Ruedenberg procedure[18] (eq 2 and 3).

$$L\varphi = \lambda \tag{2}$$

$$F_\lambda = LF_\varphi L^T \tag{3}$$

In the nondiagonal Fock matrix of the localized orbitals we have to discriminate two different types of matrix elements: the diagonal terms, $F_{\lambda,ii} = \langle\lambda_i|F|\lambda_i\rangle$, which are self-energies of localized molecular fragments, and the off-diagonal elements, $F_{\lambda,ij}$, which are a measure for the through-space interaction between the localized orbitals λ_i and λ_j. Diagonalization of selected subspaces defined by the λ_i's leads to orbitals of canonical form taking into account certain through-space interactions (the orbitals are canonical with respect to the through-space subspace).

To determine the through-bond interaction quantitatively, we need a representation ψ_i of the one-particle space in which selected localized orbitals λ_i have nonvanishing interaction elements $F_{\psi,ij}$ to orbitals that are delocalized over the whole molecule, e.g., orbitals that are canonical with respect to $N-1$ orbitals ψ_j for $j = 1 \ldots N$ with $j \neq i$. These MO's have been called precanonical molecular orbitals (PCMO).[17]

Figure 4 shows two cases where one (left) or two (right) localized fragments λ_i or λ_i and λ_j, respectively, are coupled to $N-1$ or $N-2$ precanonical orbitals ψ_k. The off-diagonal element $F_{\psi,ij}$ represents the through-space coupling. In case of **2** and **3** the interaction between the π bond and the σ frame can be elucidated by the first case (left of Figure 4). The second representation of Figure 4 (right) is appropriate to study through-space and through-bond interactions in **1**.

To obtain the forms of the precanonical Fock matrices, we delete one or two columns and rows (see Figure 4 bottom) of the localized F matrix F_λ with the exception of the diagonal elements. The resulting matrices are symbolized as $F_\lambda{}^i$ or $F_\lambda{}^{ij}$. Diagonalization of the resulting localized F matrices yields a set of eigenvectors (T_i and T_{ij} in eq 4 and 5) that can be used for the desired transfor-

$$T_i F_\lambda{}^i T_i{}^T = \epsilon_k{}^{\mathrm{PCMO}}\delta_{k,m} \tag{4}$$

$$T_{ij} F_\lambda{}^{ij} T_{ij}{}^T = \epsilon_k{}^{\mathrm{PCMO}}\delta_{k,m} \tag{5}$$

$$\psi = \begin{cases} \psi_a\psi_b \ldots \lambda_i \ldots \psi_N \\ \psi_a\psi_b \ldots \lambda_i \ldots \lambda_j \ldots \psi_N \end{cases} \tag{6}$$

$$F_\psi = T_x F_\lambda{}^x T_x{}^T \tag{7}$$

$$\text{for } x = i, ij$$

mations into the precanonical representation of the Fock matrix which is shown in eq 7. Inspection of eq 6 reveals that the sets of precanonical MO's depend on the selected λ's. Diagonalization of eq 7 leads to CMO's expressed in terms of one, two, etc. localized orbitals and $(N-1)$, $(N-2)$, etc. delocalized PCMO's. The interaction between the λ_i and ψ_j $(j \neq i)$ depends on the magnitude of the off-diagonal elements $F_{\psi,ij}$ and on the energetic separation of the diagonal self-energies.

Through-Bond and Through-Space Interaction in 1

In the following we intend to discuss the behavior (localization properties, phase relationship, and shape) of

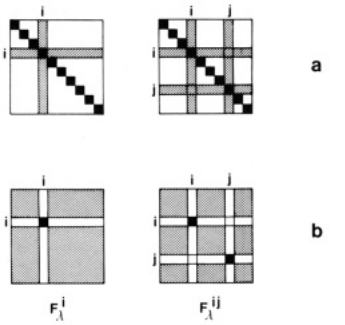

Figure 4. (a) Schematic representation of precanonical Fock matrices in which one (left) or two (right) localized fragments are coupled to $N-1$ or $N-2$ precanonical orbitals. (b) Schematic representation of the corresponding decoupled localized Fock matrices.

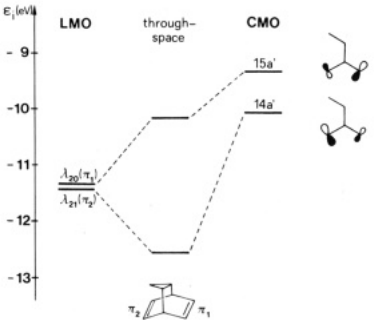

Figure 5. Correlation diagram for through-space and through-bond interaction in **1**.

	ψ_1	ψ_2	ψ_4	ψ_5	ψ_7	ψ_9	ψ_{10}	ψ_{12}	ψ_{13}	ψ_{14}	ψ_{16}	ψ_{18}	ψ_{23}	λ_{21}	λ_{20}
ψ_1	-50.44													-.42	-.14
ψ_2		-37.08												1.68	2.76
ψ_4			-32.10											-2.09	1.47
ψ_5				-26.02										-1.43	-.34
ψ_7					-22.48									-.92	.39
ψ_9						-20.60								.22	-.51
ψ_{10}							-17.69							.26	2.14
ψ_{12}								-16.03						1.72	1.23
ψ_{13}									-15.12					.38	-.06
ψ_{14}										-14.57				.68	-.30
ψ_{16}											-13.01			.93	.59
ψ_{18}												-12.79		.27	.27
ψ_{23}													-10.68	.60	.16
λ_{21}	-.42	1.68	-2.09	-1.43	-.92	.22	.26	1.72	.38	.68	.93	.27	.60	-11.40	-1.21
λ_{20}	-.14	2.76	1.47	-.34	.39	-.51	2.14	1.23	-.06	-.30	.59	.27	.16	-1.21	-11.33

Figure 6. PCMO matrix of **1**.

the two highest occupied CMO's, 15a′ and 14a′ of homobarrelene (**1**). Our calculations are based on the modified INDO model[12] since it reproduces the PE results quite satisfactorily. The Edmiston–Ruedenberg localization procedure[18] applied to the CMO's of **1** leads to the two localized π orbitals $\lambda_{20} \equiv \pi_1$ and $\lambda_{21} \equiv \pi_2$ with the following self-energies: $F_{\lambda,20} = -11.33$ eV and $F_{\lambda,21} = -11.40$ eV. The interaction parameter is found to be -1.21 eV. The diagonalization of the 2×2 matrix (eq 8) yields the following

$$\begin{vmatrix} -11.34 - \epsilon & -1.21 \\ -1.21 & -11.40 - \epsilon \end{vmatrix} = 0 \tag{8}$$

energies and coefficients for the two orbitals which show only through-space coupling:

$$\epsilon_1 = -10.16 \text{ eV}; \; c_{\pi_1} = -0.70; \; c_{\pi_2} = 0.72$$

$$\epsilon_2 = -12.59 \text{ eV}; \; c_{\pi_1} = 0.72; \; c_{\pi_2} = 0.70$$

Due to the through-space interaction between π_1 and π_2

(17) Heilbronner, E.; Schmelzer, A. *Helv. Chim. Acta* **1975**, *58*, 936.
(18) Edmiston, C.; Ruedenberg, K. *Rev. Mod. Phys.* **1963**, *35*, 457; *J. Chem. Phys.* **1965**, *43*, 597.

Table II. Decomposition of the Two Highest Occupied Canonical MO's (15a′ and 14a′) of 1 into Contributions from PCMO's ψ_i (in Percent)

ψ_i	15a′	14a′
20 (π_1)	49.91	12.96
21 (π_2)	37.91	40.77
23	5.62	28.97
10	1.83	3.69
14	1.57	0.01
4	1.09	0.01
16	0.63	5.93
12	0.47	5.58
7	0.45	<0.01
13	0.28	0.04
5	0.23	0.21
9	0.17	0.06
2	0.03	0.77
18	0.01	0.99
1	0.01	<0.01

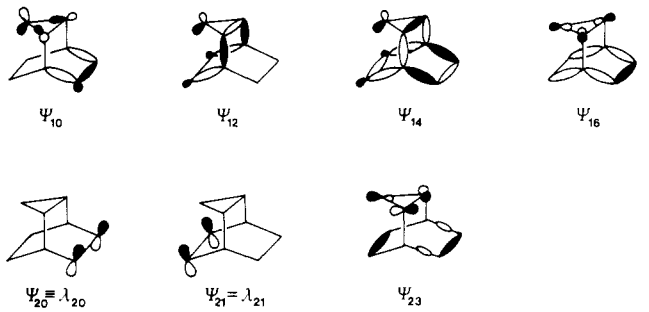

Figure 7. Schematic representation of the most important PCMO's of 1.

the two π functions are separated by 2.43 eV (center of Figure 5). The influence of the C–C σ orbitals is shown in the PCMO matrix displayed in Figure 6. The diagonalization of this matrix yields CMO's expressed as a linear combination between the two localized π orbitals λ_{20} and λ_{21} and the delocalized one-electron functions ψ_i. As displayed in Figure 5, the lower in-phase π combination, λ_{21}, is destabilized by 2.49 eV due to the σ/π interaction while the out-of-phase linear combination λ_{20} is shifted only by 0.85 eV.

The origin of this difference is revealed in Table II where the contributions of the PCMO's to the CMO's 15a′ and 14a′ are collected. It is seen that in 15a′ a π contribution of 88% is found in contrast to the 54% calculated for 14a′. It is interesting to note that the HOMO is predominantly localized at π_1 (50%) while 14a′ is mainly localized at π_2. In Figure 7 the most important PCMO's of 1 are displayed. It is seen that ψ_{23} and ψ_{16} show strong contributions localized in the three-membered ring, while the other ψ_j functions are delocalized along the C–C and C–H bonds.

A detailed investigation of the computational predictions collected in Figure 6 and Table II reveals two interesting consequences of the interactions (through-bond, through-space) present in 1: (1) The PCMO ψ_{23} mixes more strongly with λ_{21} in 14a′ than with λ_{20} in 15a′ (Table II) although the interaction element $F_{\psi,ij}$ between ψ_{23} and λ_{20} is calculated to be 0.60 eV while the one between ψ_{23} and λ_{21} is found to be only 0.16 eV (see Figure 6). This apparent discrepancy is due to the larger energy separation between the basis orbital energies for ψ_{23} and λ_{20} compared with those for ψ_{23} and λ_{21} (see Figure 6). (2) The PCMO's of σ type show nonvanishing LCAO coefficients at the carbons of the double bonds. This in turn leads to deformations due to π/σ interactions. In 15a′ only a small amount of σ contribution is predicted in contrast to 14a′. A schematic representation of both CMO's is shown in Figure 5 (right).

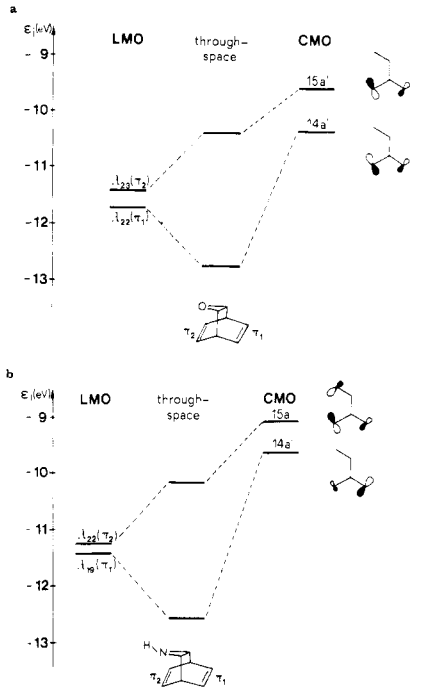

Figure 8. Correlation diagram for through-space and through-bond interaction in (a) 6 and (b) 7.

Table III. Decomposition of the Two Highest Occupied Canonical MO's (15a′ and 14a′) of 6 and 7 into Contributions from PCMO's ψ_i (in Percent)

	6			7	
ψ_i	MO_{23} (15a′)	MO_{22} (14a′)	ψ_i	MO_{23} (15a′)	MO_{22} (14a′)
22 (π_2)	48.96	32.13	22 (π_2)	54.57	0.17
20 (π_1)	41.45	26.14	19 (π_1)	17.59	44.61
21	2.52	7.52	23	19.79	39.84
15	1.89	5.70	10	2.34	0.05
11	1.40	5.05	21	2.08	6.03
12	1.08	4.68	12	1.49	0.05
4	0.96	0.04	4	0.68	0.37
23	0.72	16.15	13	0.64	0.55
8	0.48	0.13	9	0.28	0.08
2	0.23	0.43	2	0.27	0.10
5	0.17	0.64	8	0.14	0.44
14	0.11	0.41	17	0.08	1.12
1	<0.01	0.03	5	0.02	0.48
16	<0.01	0.70	14	0.01	6.09
9	<0.01	0.24	1	<0.01	<0.01

A similar σ/π interaction with the consequence of bending of the π lobes has been discussed in the case of nonbornadiene.[19]

Extension to Related Molecules

If the methylene bridge in 1 is replaced by an O or NR unit we obtain the hetero derivatives 6 and 7, respectively. If we apply the same analysis just described to elucidate the through-space and through-bond interactions in 6 and 7, we obtain the results shown in Figure 8. As long as through-space interaction effects are considered only, similar behavior for all three compounds (1, 6, and 7) is predicted. If through-bond interaction is taken into account, however, the frontier orbitals of all three compounds show remarkable differences. In Table III we have listed the most important precanonical MO's that contribute to the highest occupied molecular orbitals (15a′ and 14a′) of

(19) Böhm, M. C.; Carr, R. V.; Gleiter, R.; Paquette, L. A. *J. Am. Chem. Soc.* **1980**, *102*, 7218.

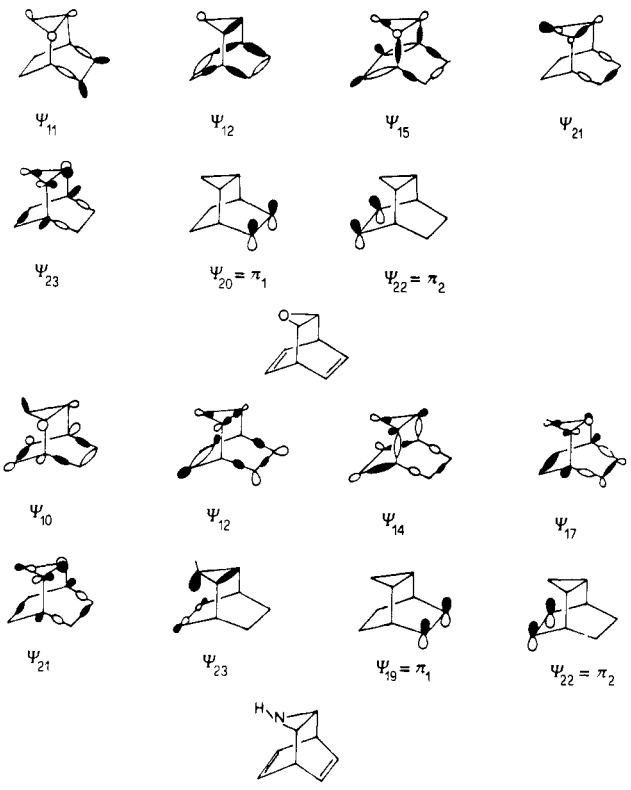

Figure 9. Schematic representation of the most important PCMO's of 6 and 7.

6 and 7. In Figure 9 the most important precanonical MO's of 6 and 7 are shown schematically.

In comparing the results of Tables II and III, we notice that the HOMOs of 6 and 7 are predominantly localized at π_2 in contrast to 1 where the HOMO is localized at π_1. For 14a' we notice in all three cases a stronger π/σ mixing.

In the case of 6 the PCMO ψ_{23} is of Walsh type and is related to $6a_1$ (HOMO) of the ethylene oxide[20] (see Figure 9). The PCMO ψ_{21} can be looked at as the oxygen lone pair related to $5a_1$ of ethylene oxide.[20] The remaining PCMO's of 6 are linear combinations of the CC and CH σ bonds.

The precanonical MO ψ_{23} for 7 shows a large coefficient at the nitrogen atom and is related to 8a' of ethyleneamine.[20] Large coefficients are also found for ψ_{21}, the symmetric Walsh orbital of the ethyleneamine part, and ψ_{14}, a σ orbital.

Regioselectivities in Cycloaddition Reactions of 1, 6, and 7

In Scheme I we have collected the major products obtained from cycloaddition reactions of 1, 6, and 7 with carbenes, "oxene", and nitrene. This scheme clearly shows a directing effect of the bridging atom or group toward the attacking electrophile. In principle four different products are possible: two for attack of π_1 syn or anti to the cyclopropano moiety and two for attack of π_2, again syn or anti to the three-membered-ring fragment.

As cycloaddition reactions between a carbene and a double bond have been investigated theoretically in great detail,[21-23] only a short and qualitative analysis is given.

Scheme I

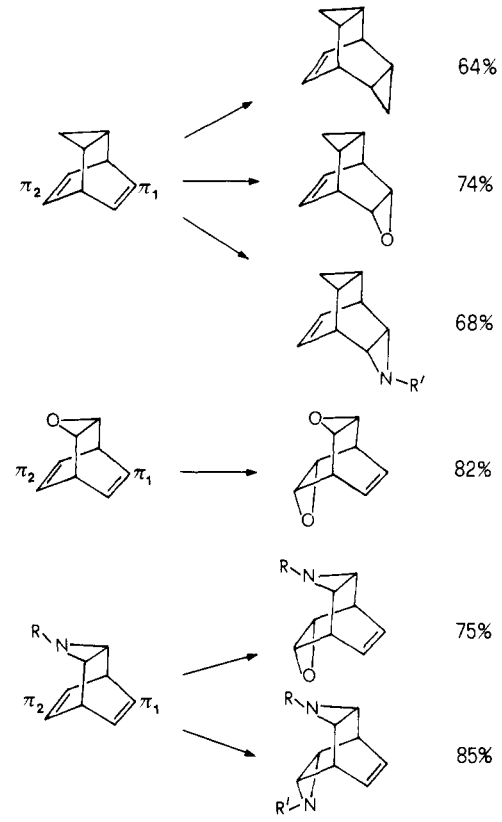

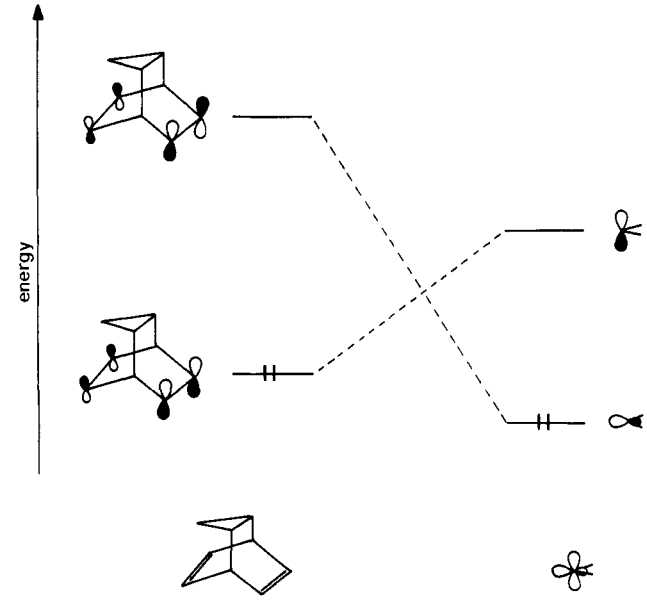

Figure 10. Interaction diagram for the frontier orbitals of 1 and a carbene.

Table IV. Localization Properties of the LUMO (9a'') of 1, 6, and 7

	1	6	7
π_1	56.16	74.81	65.00
π_2	38.49	20.74	30.69

The extension of the carbene case to the oxygen and nitrene addition uses the same arguments.

As shown in Figure 10 the cycloaddition between a carbene and a double bond, say π_1 of 1, is determined by

(20) Basch, H.; Robin, M. B; Kuebler, N. A; Baker, C.; Turner, D. W. *J. Chem. Phys.* **1969**, *51*, 58. Lathan, W. A.; Radom, L.; Hariharan, P. C.; Hehre, W. J.; Pople, J. A. *Top. Curr. Chem.* **1973**, *40*, 1.

(21) Hoffmann, R. *J. Am. Chem. Soc.* **1968**, *90*, 1475. Hoffmann, R.; Hayes, D. M.; Skell, P. *J. Phys. Chem.* **1972**, *76*, 664.

(22) Bodor, N.; Dewar, M. J. S.; Wasson, J. S. *J. Am. Chem. Soc.* **1972**, *94*, 9095.

(23) Schoeller, W. W.; Yurtsever, E. *J. Am. Chem. Soc.* **1978**, *100*, 7548. Schoeller, W. W.; Brinker, U. H. *Z. Naturforsch., B: Anorg. Chem., Org. Chem.* **1980**, *358*, 475.

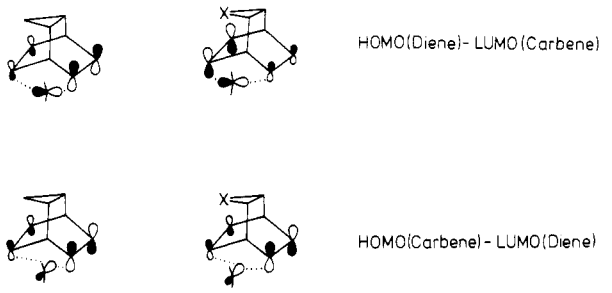

Figure 11. Secondary orbital interactions between the frontier orbitals of 1, 6, and 7 and a carbene.

two frontier orbital interactions.[21-23] By use of arguments from simple perturbation theory,[24] the interaction between the occupied π orbital of 1 and the empty 2p orbital of the carbene exceeds the interaction between the HOMO of the carbene (σ) and the LUMO (π^*) of the olefin. The preference for $\pi/2p$ over π^*/σ is due to the smaller energy separation between π and 2p orbital. For 1 the carbene has the choice between π_1 and π_2. The cycloaddition will take place at that double bond where the overlap between $\pi/2p$ and σ/π^* is largest. To find this out, we have listed in Table IV the localization properties of the LUMO (9a″) of 1, 6, and 7. From these values and the data for the HOMO (Table II) it is easy to rationalize the observed preference for the attack at π_1.

The anti attack at π_1 is the result of a secondary interaction between the frontier orbitals of the carbene and π_2 as shown in Figure 11. This secondary interaction leads to an additional stabilization of the anti-π_1 transition state.

In case of 6 the HOMO is predominantly localized at π_2 (see Table IV and Figures 8a and 11) which explains the product distribution (Scheme I). The anti attack at π_2 again results from a secondary interaction between the empty 2p orbital of the carbene and the HOMO of the π system as well as the LUMO of the π system and the occupied σ orbital of the carbene (see Figure 11).

For the ethyleneamine system 7 a consideration of the HOMO (see Figures 8 and 11) explains the attack at π_2. In contrast to 1 and 6, however, the syn attack on π_2 seems at least as likely as the anti attack since for both approaches we encounter a stabilization of a 2p acceptor due to a secondary interaction as shown below. Decisive for

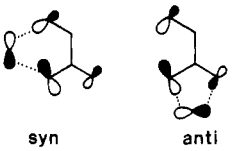

anti attack is the additional stabilization between the HOMO (σ) of the carbene and the LUMO of the π system which results for anti but not syn attack on π_2 (see Figure 11). In the case of syn attack on π_2 the σ/π interaction just discussed is strongly antibonding. Finally, it should be mentioned that the reactions just discussed are nice examples that homoconjugation *is* important as soon as nearly degenerate π levels are involved.[28]

Experimental Section

The preparation of the hydrocarbons 1–4 has been reported.[25] The oxa (6) and aza (7) analogues of homobarrelene have been obtained by epoxidation of barrelene (5)[26,27] and nitrene addition to 5, respectively.[27]

The PE spectra of 1–4 were recorded on a PS 18 spectrometer (Perkin-Elmer, Ltd., Beaconsfield, England). The purity of the compounds was examined by GC and mass spectrometry. The calibration was done with Xe and Ar. A resolution of 20 meV was achieved with the $^2P_{3/2}$ Ar line.

Registry No. 1, 7092-05-9; 2, 27335-51-9; 3, 27367-72-2; 4, 70469-89-5.

(24) Heilbronner, E.; Bock, H. "Das HMO-Modell und seine Anwendung"; Verlag Chemie: Weinheim/Bergstr., Germany; 1970. Dewar, M. J. S.; Dougherty, R. C. "The PMO Theory of Organic Chemistry"; Plenum Press: New York, 1975.

(25) de Meijere, A.; Weitemeyer, C.; Schallner, O. *Chem. Ber.* **1977**, *110*, 1504.

(26) Weitemeyer, C.; de Meijere, A. *Angew. Chem.* **1976**, *88*, 721; *Angew. Chem., Int. Ed. Engl.* **1976**, *15*, 686.

(27) Preuss, T. Ph.D. Dissertation, University of Hamburg, 1982.

(28) Bischof, P.; Gleiter, R.; Heilbronner, E. *Helv. Chim. Acta* **1970**, *53*, 1425. Paquette, L. A. *Angew. Chem.* **1978**, *90*, 114; *Angew Chem., Int. Ed. Engl.* **1978**, *17*, 106.